Advanced Time–Frequency Mutual Information Measures for Condition-Based Maintenance of Helicopter Drivetrains

David Coats, *Student Member, IEEE*, Kwangik Cho, *Student Member, IEEE*, Yong-June Shin, *Member, IEEE*, Nicholas Goodman, Vytautas Blechertas, and Abdel-Moez E. Bayoumi

***Abstract*—A new concept of nonparametric signal detection and classification technique is proposed using mutual information measures in the time–frequency domain. The time–frequency-based self-information and mutual information are defined in terms of the cross time–frequency distribution. Based on time–frequency mutual information theory, this paper presents applications of the proposed technique to real-world vibration data obtained from a dedicated condition-based-maintenance experimental test bed. Baseline, unbalanced, and misaligned experimental settings of helicopter drivetrain bearings and shafts are quantitatively distinguished by the proposed techniques. With imbalance quantifiable by variance in the in-phase mutual information and misalignment quantifiable by variance in the quadrature mutual information developed and presented herein, machine health classification can be accomplished by use of statistical bounding regions.**

***Index Terms*—Aerospace components, electromechanical systems, information entropy, military aircraft, mutual information, prognostics and health management, vibration measurement.**

I. Introduction

THE STANDARD maintenance practices in military aviation involve replacing existing parts after a certain time period or a certain number of operational hours. This practice is called time-based maintenance (TBM) and can lead to failures in critical parts due to unexpected wear, causing operational downtime and potential safety hazards [1]. Therefore, instead of TBM, it is desirable to consider use-based maintenance practices so that critical parts are replaced or repaired before their full lifetimes for economic and safe operations [2]. A new practice of condition-based maintenance (CBM) is proposed for military aviation fleet management which involves changing the time- and reaction-based maintenance schedules into ones that are predictive and proactive [3], [4]. However, to achieve this innovative maintenance practice, data must be collected from vital operational components and analyzed in order to determine the current (diagnostic) and future (prognostic) health of critical components.

In order to monitor the health status of the systems, a variety of signals are collected, including vibration [5], [6], acoustic [7], and temperature. Over the past decade, great advancements have been made in health diagnostics and vibration management in military helicopters. The successes to date have resulted in the large-scale deployment of increasingly useful health-monitoring systems such as health- and usage-monitoring systems (HUMS) using Vibration Management Enhancement Program (VMEP) hardware, which have generated a wide range of benefits from increased safety to reduced maintenance costs.

Most CBM tools such as HUMS for Apache and Blackhawk helicopters assist machinery maintainers in identifying faulted components through the use of simple interfaces and indicators. The most commonly utilized functions are condition indicators (CIs), which output a dimensioned or dimensionless single scalar value to monitor key factors most frequently related to frequency analysis of vibration signature. CIs need not be based upon vibration analysis alone and may include component temperatures or acoustic data for separate or fused CIs. Examples of common indicators in machine diagnostics and prognostics include the following: spectral peak analysis, envelope analysis, energy ratio, crest factor, sideband index, and kurtosis of residual signals [8]. These CI values are typically compared with preestablished thresholds in a simple decision tree classifier which assign the CI with some form of ranked class such as "good," "caution," or "exceeded," and these classes are then utilized by maintainers in vital decision-making processes. A given component can have several CIs which may additively form a health indicator (HI). Typically, CIs or HIs are not fault specific; multiple fault types can affect the value of a single CI, and a single fault could affect multiple CIs.

While various CIs and HIs do exist, we aim to improve their effectiveness by developing new general methods for fault

Manuscript received March 17, 2010; revised September 20, 2010; accepted November 12, 2010. This work was supported in part by the South Carolina Army National Guard, by the United States Army Aviation and Missile Command via the Condition-Based Maintenance Research Center, Department of Mechanical Engineering, University of South Carolina, Columbia, and by the National Science Foundation under Grant 0747681, "CAREER: Diagnostics and Prognostics of Electric Cables in Aging Power Infrastructure." The work of D. Coats was supported by a National Science Foundation Graduate Research Fellowship Program. The Associate Editor coordinating the review process for this paper was Dr. Jiong Tang.

D. Coats and Y.-J. Shin are with the Department of Electrical Engineering, University of South Carolina, Columbia, SC 29208 USA (e-mail: shinjune@cec.sc.edu).

K. Cho is with the Republic of Korea Army, Yongsangu, Seoul 140-701, Korea.

N. Goodman, V. Blechertas, and A.-M. E. Bayoumi are with the Condition-Based Maintenance Research Center, Department of Mechanical Engineering, University of South Carolina, Columbia, SC 29208 USA.

Color versions of one or more of the figures in this paper are available online at http://ieeexplore.ieee.org.

Digital Object Identifier 10.1109/TIM.2011.2122370

analysis based around time-frequency analysis that could be used in existing or new CIs for indication of machinery failure. Previous studies on CBM from diverse applications [9], [10] have shown that abnormality of the system is characterized by transient precursors in the signals. Through their use in detecting transient precursors, advanced signal processing techniques have contributed to develop diagnostics and prognostics algorithms for aging aircraft [11]. The classical methods for vibration analysis such as spectral analysis or time-frequency distributions represent frequency- or time- and frequency-localized energy; however, it is not an easy task to analyze multiple signals that have been simultaneously collected from systems under test. In particular, time-frequency analysis is useful to analyze the transient signature of the abnormality and its precursors [12]. Previous convention dictated that time-frequency-based applications were difficult to implement in real time; however, methods [13] have been proposed to accomplish time-frequency algorithms that are feasible for the constant monitoring required for CBM [14]. We present a path toward using time-frequency analysis and specify metrics based on time-frequency representations for condition and health monitoring, advancing the analysis of data from existing condition-monitoring systems without the use of additional hardware.

In this paper, we propose a new concept of nonparametric detection and classification of signals. We define time-frequency-based self-information and mutual information in order to classify the health status of the system components in Section II. Other methods [6], [15], [16] have been proposed to use either classical methods or neoclassical methods, moving toward the use of both time- and frequency-based information. The proposed method takes advantage of both time- and frequency-domain transients to establish a complexity measurement for potential assessment of component health. The experimental setup and data description are provided in Section III. The results and discussions are provided in Section IV, and conclusions of this paper are drawn in Section V. Based on the time-frequency-based mutual information theory, this paper presents applications of the proposed technique to real-world vibration data.

II. Time–Frequency Information Measure

The classical information measure of a continuous stochastic process is known as Shannon information [18] given as

$$H_x = -\int_{-\infty}^{\infty} f(x)\log_2 f(x)\,dx \tag{1}$$

where the continuous function $f(x)$ is a probability density function which is positive and bounded between zero and one. Williams *et al.* [18] proposed a measure of time-frequency information by use of the generalized Rényi information. The definition of the generalized Rényi information [19] of a continuous bivariate distribution $P(x,y)$ is defined as follows:

$$H_\alpha(P) = \frac{1}{1-\alpha}\log_2\frac{\int\int P^\alpha(x,y)\,dx\,dy}{\int\int P(x,y)\,dx\,dy}. \tag{2}$$

The definition of the generalized Rényi information can be extended by replacing the bivariate distribution $P(x,y)$ with a Cohen class [20] time-frequency distribution $C_s(t,\omega)$ of signal $s(t)$ with the following definition:

$$C_s(t,\omega;\phi) = \frac{1}{4\pi^2}\iiint s^*\left(u-\frac{\tau}{2}\right)s\left(u+\frac{\tau}{2}\right) * \phi(\theta,\tau)e^{-j\theta t-j\tau\omega+j\theta u}\,d\theta\,d\tau\,du. \tag{3}$$

The use of the Cohen class distribution permits a more general solution, allowing for variable kernel selection. The kernel function of the distribution is described by the $\phi(\theta,\tau)$ term in (3). In other words, the theory described in this section presents analysis for the general case of the Cohen class time-frequency distribution, while any distribution kernel could be selected when applying the time-frequency mutual information measure, including, but not limited to, the general (Cohen class), spectrogram, Zhao–Atlas-Marks, Wigner-Ville, Choi-Williams, or reduced interference distribution kernel [20]. In this paper, we selected the spectrogram kernel for the time-frequency information because it has the desirable property of nonnegativity forwarded by Williams *et al.* in [18] for all time and frequency variables. To provide consistency of discussion with time-frequency analysis in Section III-C, the spectrogram here is defined as a Cohen class distribution as seen in (3), where the kernel function $\phi(\theta,\tau)$ is specified as the spectrogram kernel given by

$$\phi(\theta,\tau) = \int h^*\left(u-\frac{1}{2}\tau\right)h\left(u+\frac{1}{2}\tau\right)e^{-j\theta u}\,du. \tag{4}$$

In addition, the spectrogram is a distribution that warrants positivity for all time and frequency variables, which is a desirable quality for the bivariate distribution described by $P(x,y)$ in (2) and another reason why we selected the spectrogram for use in this paper.

The order of the generalized Rényi information determined by parameter α for the time-frequency distribution has been investigated in [21] so that $\alpha = 3$ is a reasonable selection, with the exception of contrived counterexamples [18]. Hence, the following information measure of the time-frequency distribution will be utilized in this paper:

$$H_\alpha(C_s) = \frac{1}{1-\alpha}\log_2\frac{\int\int C_s^\alpha(t,\omega)\,dt\,d\omega}{\int\int C_s(t,\omega)\,dt\,d\omega}. \tag{5}$$

The metric $H_\alpha(C_s)$ defined in (5) measures the number of signal elements of $s(t)$ over the time and frequency planes. The Rényi information measure is a meaningful measure of the time-frequency distribution, but it is only defined for a single realization of a signal, e.g., self-information. If we have a pair of signals closely related, how can we define or quantify the interactions in terms of information? We will investigate a generalization of the time-frequency information measure by introducing the mutual time-frequency information.

In order to analyze the information of two closely spaced components, the classical mutual information of two random processes is extended to two time-frequency distribution functions. Let us consider the classical definition of the mutual information that might be extended to the measure of mutual information of the time-frequency distributions. The joint entropy

$H(X,Y)$ of a pair of continuous random variables (X,Y) with a joint probability density function $p(x,y)$ is defined as

$$H(X,Y) = -\int\int p(x,y)\log_2 p(x,y)\,dx\,dy. \tag{6}$$

By chain rule

$$H(X,Y) = H(X) + H(Y|X) \tag{7}$$

where $H(Y|X)$ is the conditional entropy. Under the same conditions, the mutual information $I(X;Y)$ is the relative entropy between the joint distribution $p(x,y)$ and the product distribution of the individual marginal distributions $p(x)$ and $p(y)$ as follows:

$$I(X;Y) = \int\int p(x,y)\log_2 \frac{p(x,y)}{p(x)\cdot p(y)}. \tag{8}$$

The relation of the mutual information $I(X;Y)$ and the joint entropy $H(X,Y)$ is defined as follows:

$$\begin{aligned} I(X;Y) &= H(X) - H(X|Y) \\ &= H(Y) - H(Y|X) \\ &= H(X) + H(Y) - H(X,Y). \end{aligned} \tag{9}$$

Thus, it is necessary for us to define the cross time-frequency distribution $J_{s_1s_2}(t,\omega;\phi)$ of the signal pairs S_1 and S_2 [22]

$$\begin{aligned} J_{s_1s_2}(t,\omega;\phi) = \frac{1}{4\pi^2}\int\int\int s_1\left(u+\frac{\tau}{2}\right)s_2^*\left(u-\frac{\tau}{2}\right) \\ \times \phi(\theta,\tau)e^{-j\theta t - j\tau\omega + j\theta u}\,d\theta\,d\tau\,du. \end{aligned} \tag{10}$$

The kernel $\phi(\theta,\tau)$ is equivalent to the kernel given in Cohen's class in (3), and the cross time-frequency distribution satisfies the time and frequency marginal property under the same constraints given in Cohen's class. Consider a joint information of the time-frequency distribution $H_\alpha(J_{s_1s_2})$ in terms of the cross time-frequency distribution $J_{s_1s_2}(t,\omega;\phi)$ as follows:

$$\begin{aligned} H(S_1,S_2) &= H_\alpha\left(J_{s_1s_2}\right) \\ &= -\frac{1}{-\alpha}\log_2\frac{\int\int J_{s_1s_2}^\alpha(t,\omega)\,dt\,d\omega}{\int\int J_{s_1s_2}(t,\omega)\,dt\,d\omega}. \end{aligned} \tag{11}$$

However, one must be careful in defining the information measure of the cross time-frequency distribution which is a complex number. In addition, normalization of the distribution is important for a proper bound of the information measure. Therefore, instead of direct application of the generalized Rényi information, consider the normalized cross time-frequency distribution $\overline{J}_{s_1s_2}(t,\omega)$ as follows:

$$\begin{aligned} \overline{J}_{s_1s_2}(t,\omega) &= \frac{J_{s_1s_2}(t,\omega)}{\sqrt{C_{s_1}(t,\omega)\cdot C_{s_2}(t,\omega)}} \\ &= \frac{R_{s_1s_2}(t,\omega)}{\sqrt{C_{s_1}(t,\omega)\cdot C_{s_2}(t,\omega)}} \\ &\quad + j\frac{Q_{s_1s_2}(t,\omega)}{\sqrt{C_{s_1}(t,\omega)\cdot C_{s_2}(t,\omega)}} \\ &= \overline{R}_{s_1s_2}(t,\omega) + j\overline{Q}_{s_1s_2}(t,\omega). \end{aligned} \tag{12}$$

We can define the time-frequency mutual information measure of in-phase $I_\alpha^R(S_1;S_2) = -H_\alpha(\overline{R}_{s_1s_2})$ and quadrature $I_\alpha^Q(S_1;S_2) = -H_\alpha(\overline{Q}_{s_1s_2})$ as follows:

$$\begin{aligned} I_\alpha^R(S_1;S_2) &= \frac{1}{1-\alpha}\log_2\int\int R_{s_1s_2}^\alpha(t,\omega)\,dt\,d\omega \\ &\quad - \frac{1}{2}\cdot\left\{H_\alpha\left(C_{s_1}\right) + H_\alpha\left(C_{s_2}\right)\right\} \end{aligned} \tag{13}$$

$$\begin{aligned} I_\alpha^Q(S_1;S_2) &= \frac{1}{1-\alpha}\log_2\int\int Q_{s_1s_2}^\alpha(t,\omega)\,dt\,d\omega \\ &\quad - \frac{1}{2}\cdot\left\{H_\alpha\left(C_{s_1}\right) + H_\alpha\left(C_{s_2}\right)\right\}. \end{aligned} \tag{14}$$

Then, the mutual information measure $I_\alpha(S_1;S_2)$ of S_1 and S_2 is defined in terms of the in-phase time-frequency mutual information $I_\alpha^R(S_1;S_2)$ and the quadrature time-frequency mutual information $I_\alpha^Q(S_1;S_2)$ as follows:

$$\begin{aligned} I_\alpha(S_1;S_2) &= I_\alpha^R(S_1;S_2) + I_\alpha^Q(S_1;S_2) \\ &= -H_\alpha\left(\overline{R}_{s_1s_2}\right) - H_\alpha\left(\overline{Q}_{s_1s_2}\right) \\ &= H_\alpha\left(C_{s_1}\right) - H_\alpha\left(C_{s_1}|C_{s_2}\right) \\ &= H_\alpha\left(C_{s_2}\right) - \underbrace{\left(H_\alpha\left(C_{s_1},C_{s_2}\right) - H_\alpha\left(C_{s_1}\right)\right)}_{H_\alpha\left(C_{s_2}|C_{s_1}\right)} \\ &= H_\alpha\left(C_{s_2}\right) - H_\alpha\left(C_{s_2}|C_{s_1}\right). \end{aligned} \tag{15}$$

Therefore, the mutual time-frequency information $I_\alpha(C_{s_1};C_{s_2})$ is the sum of individual time-frequency information $H_\alpha(C_{s_1})$ and $H_\alpha(C_{s_2})$ and joint information $H_\alpha(C_{s_1},C_{s_2})$. For example, if $s_1(t) = s_2(t)$, then $C_{s_1} = C_{s_2}$ and $Q_{s_1s_2} = 0$ such that

$$I_\alpha\left(C_{s_1};C_{s_2}\right) = I_\alpha\left(C_{s_2};C_{s_2}\right) = H_\alpha\left(C_{s_1}\right) \text{ or } H_\alpha\left(C_{s_2}\right). \tag{16}$$

Based on the mutual time-frequency information measure, we investigate the efficacy of the proposed technique with real-world data sets. The experimental setup and data descriptions are provided in the next section.

III. Experimental Setup and Data Description

The Condition-Based Maintenance Research Center at the University of South Carolina has an AH-64 helicopter tail rotor drivetrain test stand for on-site data collection and analysis [1]. The test stand includes an ac input motor [Fig. 1(a)] rated at 400 hp to provide input drive to the configuration, a multishaft drivetrain supported by hanger bearings, flex couplings at shaft joining points, two gearboxes, and an absorption motor of matching rating to simulate the torque loads that would be applied by the tail rotor blades. The test stand, with picture provided in Fig. 1(b), was used to collect data to be used in conjunction with historic helicopter vibration data to develop the baseline of operation for the systems under test. The signals are collected during the operational run of the apparatus, including vibration data measured by accelerometers, temperature

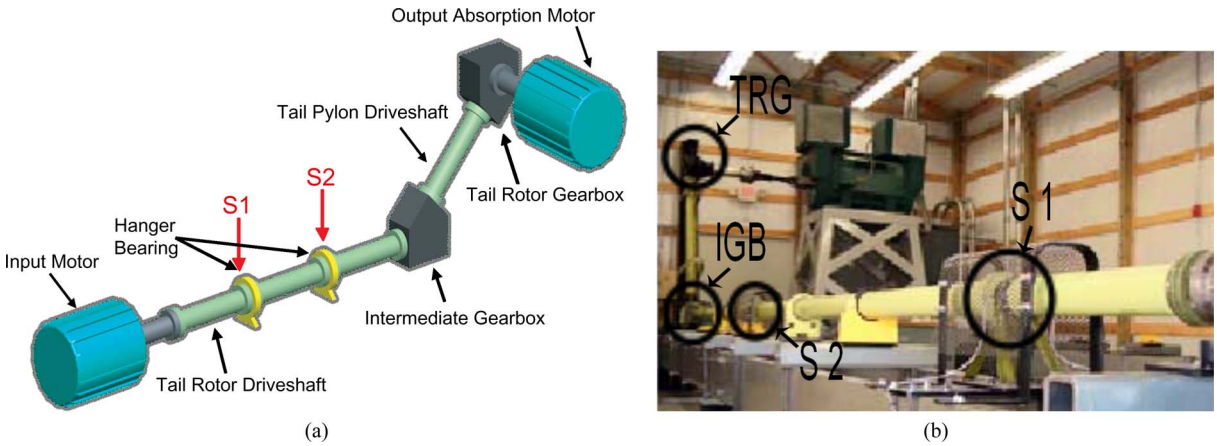

Fig. 1. Schematic representation of (a) the AH-64 helicopter tail rotor drivetrain test stand and (b) the actual test stand with labeled components for comparison.

TABLE I
LOADING PROFILE FOR A 30-min BASELINE TEST RUN

Rotational Speed (RPM)	Output Torque (ft-lb)	Input Torque (ft-lb)	Duration (min)
0-600	0	0	7.5
4863	111	32.35	30
600-0	0	0	7.5

measured via thermocouples, and speed and torque measured. The measurement devices were placed at the forward and aft hanger bearings and both gearboxes. This paper focuses on the application of time-frequency techniques to the forward and aft hanger bearing vibration signals denoted as S_1 and S_2 in Fig. 1(a) and (b). The physical separation between accelerometers (which will further be referred to more generally as sensors) on the bearings is 3.43 m.

A. Data Acquisition

The data acquisition software collects data from the hanger bearings once every 2 min during the course of the 30-min baseline runs, with the exception of two additional collection periods at the start of the run, a total of 17 measurements. An experimental run consists of an intermediate speed ramp from 0 to 600 r/min followed by a ramp from 600 to 4863 r/min. The measurements for baseline characterization were then taken during operation of the test stand at a constant rotational speed of 4863 r/min from the prime mover, with a simulation of the output torque at 111 ft · lb from the secondary. A summary of the test conditions is given in Table I given a few conventions. Rotational speed is the speed of the input shafts and hanger bearings. Output torque is given by the torque at the output of the tail rotor gearbox simulating rotor operation while the torque applied to the input shafts and hanger bearings is equal to 32.35 ft · lb.

Data collection yielded 65 536 points at a sampling rate of 48 kS/s per scheduled sampling period, which results in a data collection time of roughly 1.31 s per acquisition. For each run, data were acquired 17 times on these 1.31-s intervals: twice at the beginning and then once every 2 min until the end of the run. With individual data files containing 65 536 samples each, the acquisition results in over one million data points per set, which is too intensive for many processors to handle during time-frequency analysis. In order to resolve this computational issue and decrease the computation time, each data set under test was divided into 17 experimental frames to correspond to each time the sensor was activated to collect data. Each of the 17 experiments was then divided into 16 windows that comprised 4096 points each. Within these subdivided windows, spectrogram measurements were made on both S_1 and S_2, while the mutual information measure was applied to 4096 point segments of S_1 and S_2.

Additional windows can be determined by an overlap percentage which layers additional 4096 point windows within the main 16 windows in a given experimental frame at intervals of 4096 multiplied by the overlap percentage in order to create additional effective mutual information measurements from the given data. An overlap of 33% was determined to provide adequate clustering and enhance the probability density for implementation of predictive confidence levels.

This overlap selection helps eliminate data outliers and improve the visualization of the clustering when applying the time-frequency mutual information described in Section II to multiple data points. Therefore, the total number of mutual information measure points for the given data is equal to the number of experimental frames (17) multiplied by the number of window signal subsets (16) and the inverse of the fractional overlap percentage (3), for a total of 816 mutual points or 272 mutual points when neglecting overlap components. The data format of the time series is also provided in [14].

The configuration of the test stand uses balanced driveshafts aligned in a straight assembly as a baseline for normal operations. After performing test runs in the baseline condition, intentionally faulted configurations are tested to expand the baselines to include combinations of misaligned and unbalanced shafts. The goal of the time-frequency analysis is to establish metrics for the baseline conditions using the original data set and produce a set of metrics to diagnose each of the unbalanced and misaligned conditions. The data presented for analysis included five sets of 30-min runs of the apparatus each taken with different alignment and balancing conditions. Table II displays these conditions and their designations.

TABLE II
TAIL ROTOR DRIVESHAFT EXPERIMENTAL SETTINGS

Shaft Status	Balanced	Unbalanced
Aligned	A/B	UB/A
Misaligned	MA/B	MA/UB 3-5, 4-5

B. Misalignment and Imbalance Experimental Conditions

The primary physical fault conditions characterized experimentally are bearing imbalance and shaft misalignment. An overview of these settings helps in gaining familiarity with the experimental setup. The nomenclature of the baseline sets is dictated by numbered segments of the drivetrain. Each segment of concern in the experimentation is designated by a number (1 to 5) and coupled by flex couplings at the bearing locations to hanger bearings. Imbalance is related to driveshafts which exhibit geometrical or mass centerlines that do not coincide with axes of shaft rotation (unbalanced–aligned (UB/A) and unbalanced-misaligned (UB/MA) cases). These will be referred to as the UB/A and UB/MA cases, respectively. Misalignment (misaligned-balanced (MA/B), UB/A, and misaligned-unbalanced (MA/UB) cases) in the test configuration is characterized by a change in bearing and shaft placement that moves the number 3, 4, and 5 shafts from a straight alignment to produce an angle of 1.3°. Either a 3–5 imbalance (imbalance of three consecutive driveshafts) or a 4-5 imbalance (imbalance of only two driveshafts) differentiates two experimental settings. The aforementioned settings will be referred to as the MA/B and UB/MA 3–5 and 4-5 cases. These settings produce additional wear on drivetrain components while also presenting additional transients in harmonics that can be measured for health classification purposes. For the purposes of this paper, we will simply refer to these cases as baseline [aligned–balanced (A/B)], misaligned (MA/B), unbalanced (UB/A), and MA/UB as shown in the nomenclature in Table II. Instances of ambiguity between the MA/UB cases will be specified as 3–5 misaligned or 4-5 misaligned.

Imbalance vibrations are generated when a geometrical centerline or a mass centerline of a shaft does not coincide with the rotational axis of the shaft, for example, in cases of bearing looseness or due to manufacturing imperfections. This inconsistency between rotational axis and geometrical or mass centerline creates a radial bow force F_u at a fixed relative phase angle φ which varies in magnitude along the length of the shaft as shown in Fig. 2(b). The imbalance condition creates harmonically varying vibrations D on a hanger bearing housing, which are registered by dedicated accelerometers. These varying vibrations consist of x- and y-axis radial vibrations, z-axis axial vibrations, and torsional vibrations of a shaft in a bearing [Fig. 2(b)], as well as additional vibration signal contributions coming from coupled bearings, gearboxes, power units, airframes, and other components. Each hanger bearing on a helicopter system has only one dedicated accelerometer in current settings, which can pick only the lateral x-axis component of the vibrations [Fig. 2(c)] of the form

$$D_x = A_x \cdot \cos(\omega t + \psi_x) \tag{17}$$

$$D_y = A_y \cdot \sin(\omega t + \psi_y) \tag{18}$$

where $D_{x,y}$ and $A_{x,y}$ are the displacements and the amplitudes of the displacements in the x- and y-axis directions, ω is the angular velocity, and $\psi_{x,y}$ are the phase angles.

Vibrations caused by imbalance will be in phase on both bearing accelerometers S_1 and S_2 when $(\varphi_y - \varphi_x = 0)$ and will vary only in magnitude depending on the magnitude of imbalance F_u. The driveshaft supported by the hanger bearings at sensor locations S_1 and S_2 is not a uniform shaft but rather a sectionalized shaft as previously described. Therefore, misalignment cannot typically be avoided. It should be noted that, as shown in Table I, the experimental data are gathered under conditions of constant or near-constant torque load and speed.

Misalignment in our case is considered as an angular misalignment when the shaft centerlines of the two shafts meet at an angle with each other. This, on the contrary to imbalance, causes axial preloads on the shaft in the z-axis direction and can be decomposed to an x signal component based on the angle of misalignment $F_x = F_z \sin(\alpha_m)$. This force will have the greatest impact on the bearing closest to the shafts' coupling point and will have a phase difference in reference to force registered at a further located sensor $(\varphi_y - \varphi_x \neq 0)$ [Fig. 2(c)] because of finite stiffness and dampening in the system.

In industrial vibration monitoring, one would use shaft diagnosis techniques such as shaft centerline orbit monitoring, which requires two x and y sensors at a single location and a skilled human operator, which make such technique inapplicable in our case and justify the need for an advanced diagnostic measure. The mutual information measure takes advantage of two accelerometer signals located at different locations, simultaneously quantifying frequency and phase components of the mechanical vibration signals.

C. Analysis via Spectrogram and via Rényi Information

A Cohen class time-frequency distribution utilizing the spectrogram kernel as detailed in Section II was used to identify time-frequency signatures of different experimental setups. In Fig. 3(a) and (b), a set of spectrograms of signal S_1 is provided for the baseline shaft and the MA/UB shaft, selected for its significant increase in transient time-frequency content over the A/B case. The top portions of the figures are the time series, and the time-frequency distribution is provided in the same time axis. The classical power spectral density results are summarized in Table III with dominant frequencies common to both sensors determined by cross-power spectral density calculations between S_1 and S_2 for each experimental setting. Typical CIs measure changes in the spectra of one or more sensors based on static power spectrum plots, similar to this analysis. However, these characteristics and the key frequency harmonics, as well as transient variations in these harmonics, of the power spectral density can be visualized and summarily expressed in the spectrogram plots of S_1 and S_2. The vibration signatures in the time-frequency domain exhibit distinctive characteristics in the oscillatory nature of the system harmonics.

From analysis of the spectrograms, the existence of the dominant frequencies seen from the power spectral density and cross

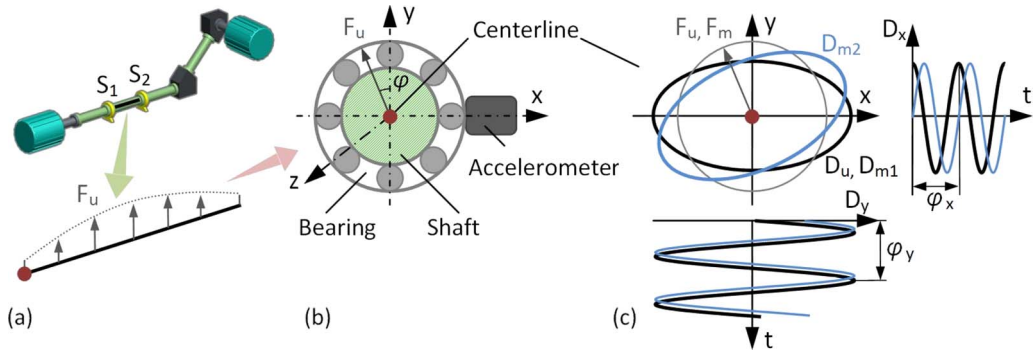

Fig. 2. Imbalance force distribution over the shaft supported at the S_1 and S_2 accelerometer locations: (a) Cross section of a bearing and the shaft at the S_1 accelerometer location, (b) shaft centerline orbits at the S_1 and S_2 accelerometer locations, and (c) displacement or vibration components in the x- and y-axis directions (D_u, D_{m1} orbits when $\varphi_y - \varphi_x = 90°$; D_{m2} orbits when $\varphi_y - \varphi_x = 120°$).

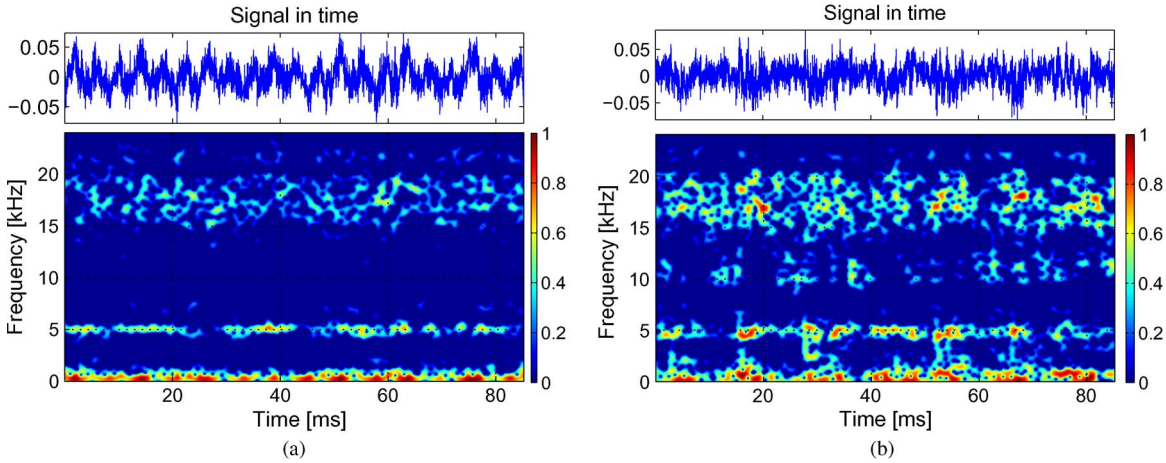

Fig. 3. Spectrogram of S_1 for (a) baseline (B/A) and (b) MA/UB (MA/UB 3–5).

TABLE III
NOMINAL FREQUENCIES AND HARMONICS IN THE TAIL ROTOR DRIVE COMPONENTS COMPARED TO DOMINANT FREQUENCIES OF THE BASELINE TESTS

Components	Nominal (Hz)	Baseline A/B (Hz)	Misaligned MA/B (Hz)	Unbalanced A/UB (Hz)	Unbalanced-Misaligned (Hz)
Tail Rotor 1R	23.40	24.2	25.0	–	–
Tail Rotor 2R	46.80	–	–	–	–
Tail Rotor Drive Shaft 1R	80.30	82.2	82.0	84.5	81.4
Tail Rotor Drive Shaft 3R	243.17	244.3	244.0	248.8	244.0/291.0
Hanger Bearing BPF 4R	1,150.19	–	1,130.0	1,347.0	1349.0
Tail Gearbox Gear Mesh	1,333.20	1,590.0	–	1,582.0	–
Tail Gearbox 2R	2,666.40	2,274.0	–	2,277.0	–
Intermediate Gearbox Gear Mesh	2,969.40	–	3,085.0	–	–
Tail Gearbox 3R	4,038.00	–	–	–	4531.0
Tail Gearbox 4R	5,384.00	5,049.0	–	5,075.00	5107.0

spectrum can be confirmed and can easily be seen as the high-density stripes on the range of 23 Hz–4 kHz. For example, two distinct frequency stripes can be seen in the aft hanger bearing readings. The higher frequency stripe of these frequency stripes (1.5- to 2-kHz range) is not found on the forward hanger bearing. This frequency stripe is attributed to frequencies emanating from the tail rotor gearbox. The major differences in the forward hanger bearing reading between the balance and imbalance cases revolve around the increases in power related to the 5- and 15–20-kHz bands. Higher frequencies, as shown in Table III, typically coincide with contributions from the intermediate and tail rotor gearbox mesh frequencies on S_2. Metal-to-metal contact of faulted machinery has been known to cause shock pulse energy and acoustic emissions near and well above the 20-kHz human auditory range, possibly coinciding with the frequency bands near 15–20 kHz; however, a sampling rate of 48 kHz limits the investigation of these frequencies.

Furthermore, the number of signal elements on the time-frequency plane can be mathematically assessed using the Rényi information measure. The Rényi information measures of the time-frequency distribution in S_1 [shown in Fig. 3(a)] and S_2 are 6.83 and 6.71 bits, respectively, using the equation

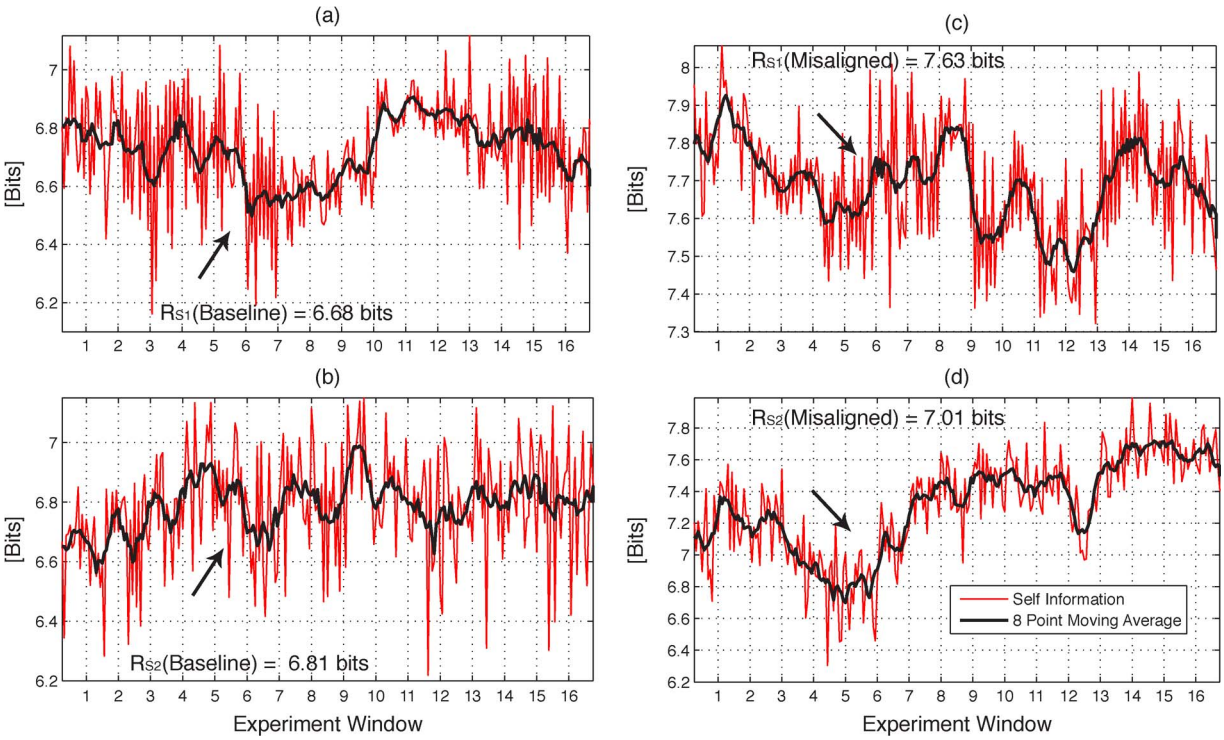

Fig. 4. Rényi self-information measures of (a) S_1 and (b) S_2 for baseline. Rényi self-information measures of (c) S_1 and (d) S_2 for misalignment.

defined in (5). One can find more time-frequency signal components in Fig. 3(a) at the 15–20-kHz frequency bandwidth, which results in a slightly higher value of the Rényi information measure of the spectrogram in Fig. 3(a). In addition, the Rényi information measures of the misaligned-case time-frequency distribution of S_1 [shown in Fig. 3(b)] and S_2 are 7.83 and 6.93 bits. Comparing the spectrograms in Fig. 3(a) and (b) illustrates that the spectrograms in Fig. 3(b) exhibit more time-frequency components than those in Fig. 3(a), and one can quantitatively confirm a reasonable measure of the time-frequency information using the Rényi information measure.

These differences and signatures on the time-frequency domain cannot be clearly distinguished from the traditional power spectrum reading, a fact which is made apparent from the quantitative reading of the Rényi information. Nevertheless, the results obtained by the spectrogram are not sufficient to describe mutual interactions between the signal pair of S_1 and S_2 in different experimental setups. In the next section, we investigate the efficacy of the time-frequency-based mutual information measure discussed in Section II in order to quantitatively characterize the experimental setups of the baseline and misaligned shafts.

IV. Results and Discussion

A. Comparison of Rényi-Derived Self-Information to Classical Time–Frequency Methods

The first step of the analysis and discussion uses the Rényi self-information measure defined in (5) to describe the individual time series. The Rényi self-information measures of S_1 and S_2 for the baseline and misaligned cases are shown in Fig. 4. Signal 1 S_1 and signal 2 S_2 in both the baseline (A/B) and misaligned (MA/B) cases are processed by applying the eight-point moving average filtering followed by Rényi information calculation to obtain the self-information measure. Thus, for every time instance of every experiment window of the data, a Rényi calculation of each autocorrelated signal was gathered. As shown in Fig. 4, a total of 272 self-information measures were gathered for each signal of each case. Additional overlapping is used for $x-y$ coordinate mapping used in visualizing part health. In order to identify the tendency of the measure, an eight-point moving average filter was applied to each signal with the filter covering half of the time instances provided in each experiment window. The results of this self-information measure are compared side by side in Fig. 4 for each signal. The referenced time instance (15th of the file frame at the 5th experiment window) is marked on each graph to show consistency with the analyses in Sections I and III-C, which use the same 4096 data points for the spectrogram.

Notable difference from the side-by-side comparison in Fig. 4 is a sizable increase in the self-information measure of the misaligned case over the baseline case. This could be a characteristic signature of a misaligned case. The self-information measure shows a general increase at the given samples when comparing the balanced–aligned (B/A) case with the misaligned case and an increase on the average of the measured frames. The average self-information value of the baseline S_1 signal is reported at 6.72 bits, while the average value of the same signal in the MA/B case was 7.68 bits. Comparing the second signal set S_2, we obtain a value of 6.78 bits compared to 7.31 bits for the same cases. However, from this derived metric, the interpretation is yet unclear. This self-information measure can be verified using the spectrogram example discussion in Fig. 3. From these data, there is little other indication of change

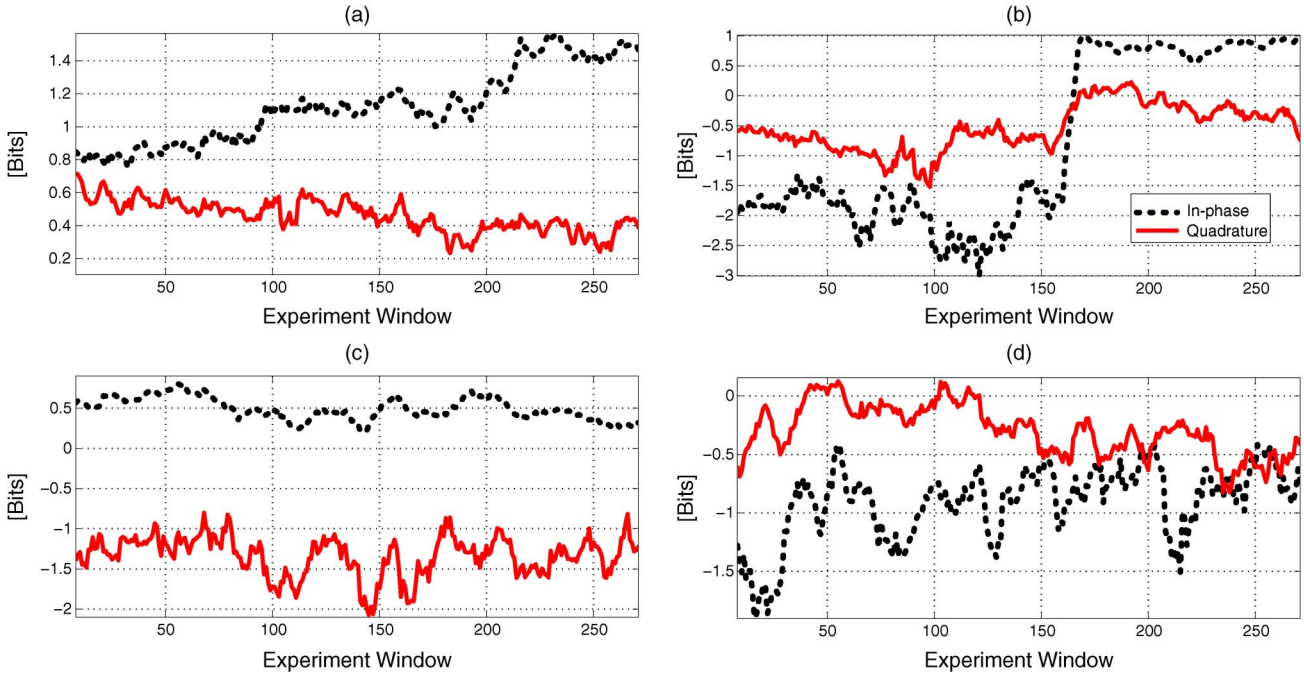

Fig. 5. Mutual Rényi information measures of S_1 and S_2 for the (a) baseline–aligned, (b) aligned-unbalanced, (c) MA/B, and (d) MA/UB cases.

from the baseline case to another "faulty" status of the shaft. Moreover, the Rényi self-information of S_1 in the balanced case in Fig. 4(a), as well as both signals in the misaligned case, oscillates more compared to the Rényi self-information of S_2 of the baseline case (A/B). This could be attributed to more high-frequency components shown in the time-frequency spectrogram in Fig. 3(b).

While this self-information proves useful and shows a notable basis by which to compare data sets, it lacks potential for comparison of closely related signals and, in this instance, shows an increase when compared on average while not for localized comparison. This only partly supports the desired qualities of a CI, while further information can be gathered from the mutual information measure. This mutual information measure is a complex value and can be further subdivided into two constituent values: an in-phase mutual time-frequency information $(I_\alpha(R_{s_1 s_2}))$ and a quadrature mutual time-frequency information $(I_\alpha(Q_{s_1 s_2}))$ defined in (13) and (14).

B. In-Phase and Quadrature Components of the Time–Frequency Mutual Information Measure

The mutual information measures of the baseline and misaligned cases are shown in Fig. 5. An interesting trend can be seen in the baseline case in Fig. 5(a). Overall, the in-phase mutual time-frequency information $(I_\alpha(R_{s_1 s_2}))$ stays mostly at a constant separation from the quadrature mutual time-frequency information $(I_\alpha(Q_{s_1 s_2}))$. Both $I_\alpha(R_{s_1 s_2})$ and $I_\alpha(Q_{s_1 s_2})$ of the baseline case in Fig. 5(a) remain relatively constant throughout all windows of the experiment. However, toward the end of the sequence outlined in Fig. 5(a), the in-phase and quadrature mutual information measure values begin to experience a larger separation. These characteristics are all important to be noted while considering what truly characterizes the baseline physics of the system.

A glance at the mutual information from the misaligned case in Fig. 5(b) draws attention to two distinctive signatures. First, like the baseline case, the cospectral mutual time-frequency information $(I_\alpha(R_{s_1 s_2}))$ remains relatively constant throughout all experiment windows with a large trough around experiment window 10 corresponding to a minimum value of the quadspectral mutual time-frequency information $(I_\alpha(Q_{s_1 s_2}))$. Second, the quadrature component has a larger average value over the length of the experiments than was seen in the quadspectral component in the baseline case. Also, the quadspectral component in the misaligned case fluctuates greatly, showing greater amounts of local minima and maxima. Although the quadspectral information in the misaligned case revealed a significant rise in the number of bits in the mutual information measure, the cospectral portion showed little increase over the experiment windows measured. By comparing the results in Fig. 5 with other results by classical spectral analysis or traditional spectrogram, one can find the usefulness of the proposed technique for a quantitative health condition assessment of the experimental setup. Further analysis is underway to understand the relationship between the time-frequency mutual information method and other confounding factors such as speed and torque, isolating the sources of transient changes in the vibration signatures.

C. Time–Frequency Mutual Information Measure Visualization and Statistical Analysis

The mutual information measure currently in development and shown in Fig. 6 provides a graphical interpretation of part condition by analyzing the amount of mutual data shared

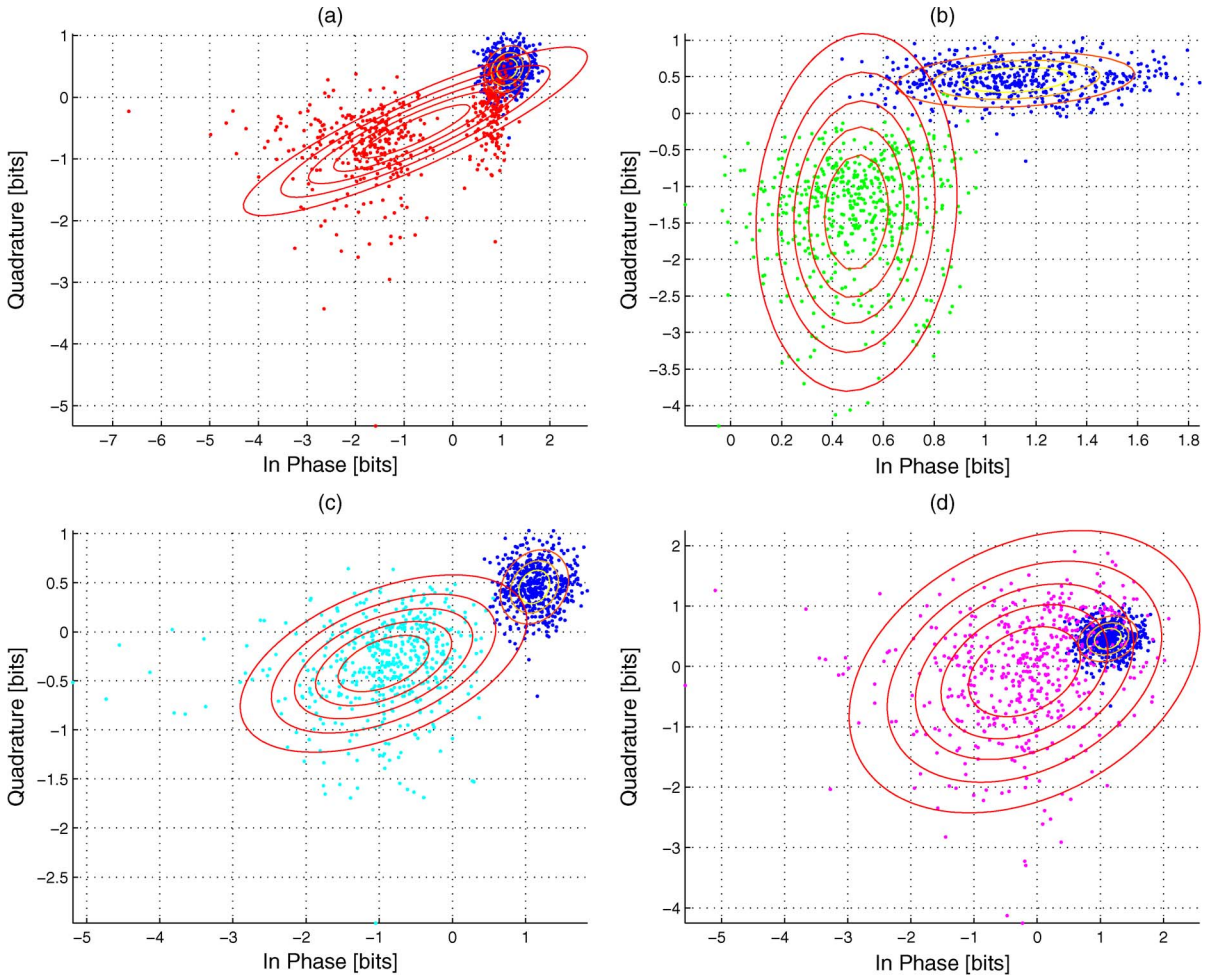

Fig. 6. Baseline comparisons of the mutual information measure: (a) Aligned-unbalanced, (b) MA/B, (c) MA/UB 3–5, and (d) MA/UB 4-5 cases with the A/B case.

between two vibration signals received from separate accelerometers. The mutual information measure is composed of a quadrature component and an in-phase component which, by observation, seem to indicate differences in the actual physics of the system. Fig. 6 shows the scatter plot distribution of the in-phase component of the measure on the x-axis and the quadrature component of the measure on the y-axis. In the condition of system imbalance, as shown in Fig. 6(a), (c), and (d), which compares the misaligned and unbalanced experimental settings to the standard baseline, the in-phase component shows a potential trend toward a decrease in information bits.

Similarly, misalignment can be observed to decrease the number of information bits of the measure contained in the quadrature component, shown in Fig. 6(b) and (d). As a distribution, these values can be seen to shift along the x–y plane, indicating a shift in part or system status. Additional studies should be analyzed and compared to determine if these trends are truly linear as they appear to be from observation. It would appear that those in Fig. 6(c) and (d), which were tested under both misalignment and imbalance conditions, as well as combination settings, have differing degrees of misalignment and imbalance, yielding different distributions which follow the established trends along the quadrature and in-phase components. Included in Table IV is reference for the statistics related to both spectra of the mutual information measure proposed. Future studies of this indicator method could focus on varying states of misalignment and imbalance to determine a quantifiable relation between the x–y distribution shift and part health. Differences in this mutual information measure could be further developed into an increased precision statistical indicator of part or system health status.

V. Conclusion

Drawing from Rényi complexity measures and mutual information theory, baseline, unbalanced, and misaligned experimental settings are quantitatively distinguished by the proposed mutual information technique. Statistical analysis of the time-frequency information measure from Table IV shows variances in the proposed in-phase and quadrature information measures of 0.0070 (STD of 0.0837) and 0.0054 (STD of 0.2324), respectively, for baseline test-bed conditions in opposition to an increased in-phase information measure variance of 3.33 (STD of 1.8258) in repeated unbalanced test cases and an increased quadrature information measure of 1.7497 (STD of 1.3228) in repeated misaligned cases. With imbalance quantifiable by variance in the in-phase mutual information and misalignment quantifiable by variance in the quadrature mutual information,

TABLE IV
STATISTICAL SUMMARY OF THE MUTUAL INFORMATION MEASURE

Statistical Parameter		Baseline	Aligned-Unbalanced	Misaligned-Balanced	Misaligned-Unbalanced 3-5	Misaligned-Unbalanced 4-5
Mean μ	*In Phase*	1.1202	-0.7424	0.4902	-0.9535	-0.1753
	Quad	0.4535	-0.5509	-1.3691	-0.3268	-0.0726
STD σ	*In Phase*	0.0837	1.8258	0.2147	1.0136	1.4344
	Quad	0.2324	0.7107	1.3228	0.4852	1.2363
Correlation ρ		0.2326	0.8732	0.0891	0.4005	0.3188

machine health classification can be accomplished using statistical bounding regions. In summary, the baseline can be characterized with a constant separation on a per-time-instance basis of the mutual information measure. The misaligned case may be characterized by its quadrature component. This component shows the misalignment in a relatively large increased number of bits from the information measure. However, similarity still remains in the in-phase component whether the case is aligned or misaligned. The authors are interested in the fusion of other types of sensors in order to obtain extended information for more accurate assessment of the health status. Data could be gathered from vibration, acoustic, and temperature sensors and correlated to present a single more robust HI [24], [25]. Furthermore, analysis of these values can yield great insights into the physics behind systems such as the system under study which provided the mechanical vibration data, providing either a simple summary of component health for an operator or a complex interpretation from a knowledgeable engineer in order to fully achieve CBM.

ACKNOWLEDGMENT

The author D. Coats would like to thank the National Aeronautics and Space Administration for the EPSCoR Undergraduate Scholarship and the University of South Carolina for the Magellan Undergraduate Scholarship. The author K. Cho would like to thank the Republic of Korea Army for the Overseas Education Scholarship.

REFERENCES

[1] A. Bayoumi, N. Goodman, R. Shah, L. Eisner, L. Grant, and J. Keller, "Integration of maintenance management systems and health monitoring systems through historical data investigation," presented at the Tech. Specialists' Meeting Condition Based Maintenance, Huntsville, AL, 2008.

[2] A. Bayoumi, N. Goodman, R. Shah, L. Eisner, L. Grant, and J. Keller, "Implementation of CBM through the application of data source integration," presented at the Tech. Specialists' Meeting Condition Based Maintenance, Huntsville, AL, 2008.

[3] A. Bayoumi, N. Goodman, R. Shah, L. Eisner, L. Grant, and J. Keller, "Examination and cost-benefit analysis of the CBM process," presented at the Tech. Specialists' Meeting Condition Based Maintenance, Huntsville, AL, 2008.

[4] A. Bayoumi, N. Goodman, R. Shah, T. Roebuck, A. Jarvie, L. Eisner, L. Grant, and J. Keller, "Aircraft components mapping and testing for CBM," presented at the Tech. Specialists' Meeting Condition Based Maintenance, Huntsville, AL, 2008.

[5] I. Santamaría-Caballero, C. J. Pantaleón-Prieto, J. Ibáñez-Díaz, and E. Gómez-Cosıacute;o, "Improved procedures for estimating amplitudes and phases of harmonics with application to vibration analysis," *IEEE Trans. Instrum. Meas.*, vol. 47, no. 1, pp. 209–214, Feb. 1998.

[6] G. Betta, C. Liguori, A. Paolillo, and A. Pietrosanto, "A DSP-based FFT-analyzer for the fault diagnosis of rotating machine based on vibration analysis," *IEEE Trans. Instrum. Meas.*, vol. 51, no. 6, pp. 1316–1322, Dec. 2002.

[7] J. Jó da Silva, A. Marcus Nogueira Lima, F. Helmut Neff, and J. Sérgio da Rocha Neto, "Non-invasive fast detection of internal fouling layers in tubes and ducts by acoustic vibration analysis," *IEEE Trans. Instrum. Meas.*, vol. 58, no. 1, pp. 108–114, Jan. 2009.

[8] P. Grabill, J. Seale, D. Wroblewski, and T. Brotherton, "iTEDS: The intelligent Turbine Engine Diagnostic System," in *Proc. 48th Int. Instrum. Symp.*, 2002, p. 6.

[9] M. Vedrines, V. Gassmann, and D. Knittel, "Moving web-tension determination by out-of-plane vibration measurements using a laser," *IEEE Trans. Instrum. Meas.*, vol. 58, no. 1, pp. 207–213, Jan. 2009.

[10] R. Yan and R. X. Gao, "Complexity as a measure for machine health evaluation," *IEEE Trans. Instrum. Meas.*, vol. 53, no. 4, pp. 1327–1334, Aug. 2004.

[11] J. Banks, T. Bair, K. Reichard, D. Blackstock, D. McCall, and J. Berry, "A demonstration of a helicopter health management information portal for U.S. army aviation," in *Proc. IEEE Aerosp. Conf.*, Big Sky, MT, 2005, pp. 3748–3755.

[12] S. Santhi and V. Jayashankar, "Time–frequency analysis method for the detection of winding deformation in transformer," in *Proc. IEEE Transm. Distrib. Conf. Expo.*, Chicago, IL, 2008, pp. 1–5.

[13] S. Rajagopalan, J. A. Restrepo, J. M. Aller, T. G. Habetler, and R. G. Harley, "Nonstationary motor fault detection using recent quadratic time frequency representations," *IEEE Trans. Ind. Appl.*, vol. 44, no. 3, pp. 735–744, May/Jun. 2008.

[14] K. I. Cho, D. Coats, J. Abrahms, N. Goodman, Y.-J. Shin, and A. Bayoumi, "Applications of time–frequency analysis for aging aircraft component diagnostics and prognostics," in *Proc. SPIE—Adv. Signal Process. Algorithms, Architectures, Implementations XVIII*, San Diego, CA, Jul. 2008, pp. 70740Y-1–70740Y-10.

[15] A. R. Scott, "Characterizing system health using modal analysis," *IEEE Trans. Instrum. Meas.*, vol. 58, no. 2, pp. 297–302, Feb. 2009.

[16] R. Yan and R. X. Gao, "Hilbert–Huang transform-based vibration signal analysis for machine health monitoring," *IEEE Trans. Instrum. Meas.*, vol. 55, no. 6, pp. 2320–2329, Dec. 2006.

[17] T. Cover and J. Thomas, *Elements of Information Theory*. New York: Wiley, 1991.

[18] W. J. Williams, M. L. Brown, and A. O. Hero, "Uncertainty, information, and time–frequency distributions," in *Proc. SPIE-Adv. Signal Process. Algorithms, Architectures, Implementations X*, 1991, vol. 1566, pp. 144–156.

[19] T.-H. Sang and W. J. Williams, "Rényi information and signal-dependent optimal kernel design," in *Proc. IEEE ICASSP*, 1995, vol. 2, pp. 997–1000.

[20] L. Cohen, "Time–frequency distributions—A review," *Proc. IEEE*, vol. 77, no. 7, pp. 941–981, Jul. 1989.

[21] R. G. Baraniuk, P. Flandrin, A. Janssen, and O. Michel, "Measuring time–frequency information content using the Rényi entropies," *IEEE Trans. Inf. Theory*, vol. 47, no. 4, pp. 1391–1409, May 2001.

[22] Y.-J. Shin, E. J. Powers, and W. M. Grady, "On definition of cross time–frequency distribution function," in *Proc. SPIE—Adv. Signal Process. Algorithms, Architectures, Implementations X*, San Diego, CA, Jul. 2000, pp. 9–16.

[23] B. Zhang, T. Khawaja, R. Patrick, G. Vachtsevanos, G. Vachtsevanos, M. E. Orchard, and A. Saxena, "Application of blind deconvolution denoising in failure prognosis," *IEEE Trans. Instrum. Meas.*, vol. 58, no. 2, pp. 303–310, Feb. 2009.

[24] M. E. Stieber, E. Petriu, and G. Vukovich, "Instrumentation architecture and sensor fusion for systems control," *IEEE Trans. Instrum. Meas.*, vol. 47, no. 1, pp. 108–115, Feb. 1998.

[25] S. C. Stubberud and K. A. Kramer, "Data association for multiple sensor types using fuzzy logic," *IEEE Trans. Instrum. Meas.*, vol. 55, no. 6, pp. 2292–2303, Dec. 2006.

David Coats (S'08) received the B.S. degree (*summa cum laude*) from the University of South Carolina, Columbia, where he is currently working toward the Ph.D. degree in electrical engineering.

His undergraduate research efforts culminated in receipt of the National Science Foundation Graduate Research Fellowship in 2010. His research interests include power electronics, condition-based maintenance in aging aircraft and aerospace components, and digital signal processing in cable diagnostics.

Mr. Coats was the recipient of the National Aeronautics and Space Administration EPSCoR Undergraduate Scholarship, the Magellan Undergraduate Scholarship, and the Valedictorian Scholars Awards.

Kwangik Cho (S'09) received the B.S. degree from the Department of Electronic Engineering, Kyonggi University, Suwon, Korea, in 1999 and the M.S. degree from the Department of Electrical Engineering, University of South Carolina, Columbia, in 2009.

He is currently a Republic of Korea (ROK) Army Major and an Army Attack Helicopter Pilot. His research interests include power electronics, wireless communication, and condition-based maintenance of military aging aircraft.

Mr. Cho was a recipient of the ROK Army Scholarship for overseas education.

Yong-June Shin (S'08–M'04) received the B.S. degree (with early completion honors) from Yonsei University, Seoul, Korea, in 1996, the M.S. degree from the University of Michigan, Ann Arbor, in 1997, and the Ph.D. degree from the Department of Electrical and Computer Engineering, The University of Texas, Austin, in 2004.

He joined the Department of Electrical Engineering, University of South Carolina, Columbia as an Assistant Professor where he was promoted to Associate Professor from 2010. His areas of research are power engineering, power electronics, with emphasis on power quality, and harmonics. His research interests include advanced signal processing theory: time–frequency analysis, wavelets, and higher order statistical signal processing. His current research interests are characterized by the application of novel digital signal processing techniques to a wide variety of important transient and nonlinear problems in science and engineering. His fields of interdisciplinary research extend to network communication engineering, measurement and instrumentation, and biomedical engineering.

Dr. Shin was a recipient of the National Science Foundation Early Faculty Career Development Award (CAREER) and a GE Korean–American Educational Commission scholarship.

Nicholas Goodman received the B.S. degree in mechanical engineering from the University of South Carolina, Columbia, in 2006, with a minor in mathematics and computer science, specializing in artificial intelligence. Following a six-month language study trip to East Asia, he has been working toward the PhD. degree in mechanical engineering, with a specialization in mathematics, at the University of South Carolina, Columbia.

He is currently investigating the development of neural network algorithms for the analysis of rotorcraft vibrations and maintenance data in support of the condition-based maintenance objectives for the U.S. Army.

Vytautas Blechertas received the B.S., M.S., and Ph.D. degrees from Kaunas University of Technology, Kaunas, Lithuania.

Since 2008, he has been a Postdoctoral Research Associate with the Condition-Based Maintenance Research Center, Department of Mechanical Engineering, University of South Carolina, Columbia. His main research activities include the diagnosis of rotating machinery by vibration and acoustic emission monitoring and their data fusion. His other research interests include piezoelectric ultrasonic motors, health- and usage-monitoring systems, nanoscale material characterization, and "smart" materials.

Abdel-Moez E. Bayoumi received the B.S. degree in mechanical engineering from Tanta University, Tanta, Egypt, the M.S. degree from Helwan University, Egypt, and the Ph.D in Mechanical and Aerospace Engineering from North Carolina State University, Raleigh.

He has over 25 years of teaching and research experience. He was a Professor of mechanical and aerospace engineering with North Carolina State University, Raleigh, the Project Manager of Hewlett-Packard Company, and a Professor of mechanical and materials engineering with Washington State University, Pullman. He is the Director of the Condition-Based Maintenance Research Center, the Director of the Biomedical Engineering Program, and a Professor of mechanical engineering with the College of Engineering and Computing, University of South Carolina, Columbia. He has been actively involved in developing strong programs in mechanical systems. His research activities have been focused in mechanical behavior of materials and design, diagnosis and prognosis of mechanical systems, and design for manufacturability.